Supporting information accompanying the following article

Chmilar SL, Luzardo AC, Dutt P, Pawluk A, Thwaites VC, and Laird RA. Caloric restriction extends lifespan in a clonal plant

Contents

Appendix A: Alternative theories of lifespan extension via caloric restriction

The idea that CR leads to increased lifespans by mediating a trade-off between survival and reproduction has support in the literature (Box 1); however, more recent critiques have provided alternative possible explanations for this phenomenon.

Overfeeding

Increased longevity via CR may simply be an artifact of domestication or overfeeding. Organisms commonly used in laboratories and experimentation (rats, mice, *D. melanogaster*, *C. elegans*, etc.) often have been in human-made environments for many generations, and exposed to different selection pressures than in natural environments. The low activity and high food intake experienced by these organisms may result in overweight, fecund, and shorter-lived lab populations. Restricting food intake through CR may simply return these animals to healthier conditions, similar to those experienced by wild counterparts, resulting in a longer lifespan (Adler & Bonduriansky, 2014; Le Bourg, 2010). A meta-analysis performed by Nakagawa et al. (2012) found that model species show lifespan-extending effects in response to CR more strongly than non-model organisms, some of which showed no effect of CR at all. They note that their results most strongly support convergent evolution to laboratory conditions as an explanation for the effects of CR.

Hyperfunction

The hyperfunction theory proposes that aging is caused by the same mechanisms as those promoting growth (Blagosklonny, 2006, 2008; Blagosklonny & Hall, 2009). In early life, growth is essential, and contributes positively to fitness. In later life, growth-promoting pathways unnecessarily continue to function, causing aging and aging-related diseases (Blagosklonny, 2006, 2008; Blagosklonny & Hall, 2009). As such, the growth- and aging-promoting mechanisms are pleiotropic, and will not be strongly selected against by natural selection due to the early-life benefit they provide (Blagosklonny & Hall, 2009) – this also connects to antagonistic pleiotropy, a major evolutionary theory of senescence (Gems & Partridge, 2013; Williams, 1957). In particular, Blagosklonny (2006, 2008) identifies the target of rapamycin (TOR) pathway as the mechanism for aging. TOR is a growth-promoting pathway, acting to promote protein synthesis, cell growth, control of the cell cycle, and inhibiting autophagy (reviewed in González et al., 2020; Loewith & Hall, 2011). When nutrients are limited, TOR (and downstream processes) is inhibited, which has been shown to extend lifespan (Anisimov et al., 2011; Bjedov et al., 2010; Fabrizio et al., 2001; Jia et al., 2004; Kapahi et al., 2004; Powers et al., 2006; Saxton & Sabatini, 2017; Vellai et al., 2003). More recently, AMP-activated protein kinase (AMPK) has been found to act opposite to TOR in molecular pathways, and may also play a role in the mechanisms of longevity extension (Chung & Chung, 2019; González et al., 2020). This theory is also important as it is one of few that explicitly link the evolution of aging with the mechanisms of aging, a concept discussed and extended by Lemaître et al. (2024).

Appendix B: Obtaining focal fronds

As noted in the main text, we obtained our focal plants (i.e., the main subjects of our experiments) through a preliminary process designed to ensure recent genealogical homogeneity, in order to reduce the potential for parental and grandparental age effects, which have been observed in previous studies (Barks & Laird, 2015). Each focal plant's great-great-grandparent was taken from the stock culture and marked with a speck of dilute, autoclaved India ink. The next offspring plant to detach (i.e., the focal plant's great-grandparent) was saved and marked, and the great-great-grandparent was discarded. This retain-discard process was then repeated an additional three times (i.e., three clonal generations of first offspring) to obtain the focal plant. Thus, all focal plants are the first-born offspring, from first-born offspring, back through three generations, ensuring genealogical homogeneity.

Appendix C: Manipulating light intensity

Light intensity was manipulated using two layers of neutral density (ND) gel sheets (cat. nos. 130, 209, 210, and, 211, LEE Filters, Burbank, CA, USA) or aluminum foil (Alcan, Mississauga, ON, Canada), depending on the treatment (Figure C1). The sheets and foil were cut into discs the size of the outer container lids (60 mm nominal diameter; Figure C1), upon which they were placed. Different disc combinations were used to obtain seven light intensity treatments, the first six of which followed a $\log_2$-series (L_1, $L_{1/2}$, $L_{1/4}$, $L_{1/8}$, $L_{1/16}$, $L_{1/32}$), such that plants in each successive treatment received, putatively, half the light intensity as those in the preceding treatment, with the subscript in the treatment name referring to its light intensity relative to the 'full light' treatment:

- L_1 ('full light') had an ND 0.0 (clear) filter above another ND 0.0 filter;
- $L_{1/2}$ had an ND 0.0 filter above an ND 0.3 filter;
- $L_{1/4}$ had an ND 0.0 filter above an ND 0.6 filter;
- $L_{1/8}$ had an ND 0.0 filter above an ND 0.9 filter;
- $L_{1/16}$ had an ND 0.6 filter above another ND 0.6 filter;
- $L_{1/32}$ had an ND 0.6 filter above an ND 0.9 filter.

The seventh light intensity treatment, L_0, was a 'no light' treatment; it had an ND 0.0 filter above a disc of aluminum foil.

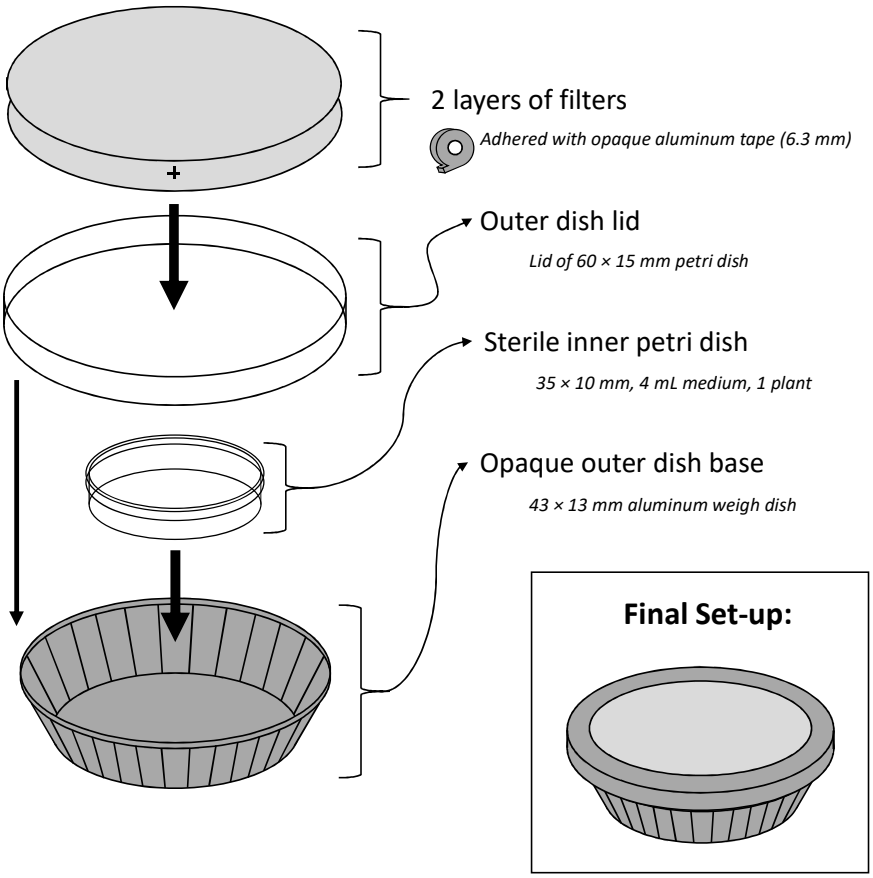

Figure C1. Schematic diagram of the set-up of the containers that housed individual *Lemna* plants (not to scale). Plants were grown in 4 mL of one-quarter (0.8 g L^{-1}) strength Schenk and Hildebrandt growth medium inside a 35 mm diameter (nominal) petri dish. This was placed, in turn, in an outer container whose base was a 43 mm diameter (nominal) aluminum weigh dish and whose lid was the lid of a 60 mm diameter (nominal) petri dish. Two discs were affixed to the top of the outer lid using 6.3 mm aluminum foil tape. In the case of light intensity treatments L_1 to $L_{1/32}$, these discs were neutral density (ND) filters; in the case of light intensity treatment L_0, the upper disc was an ND filter and the lower disc was a circle of aluminum foil.

Appendix D: Measured light intensity as a function of light intensity treatment

Methods

To investigate how light intensity was modified by the treatments, we conducted an ancillary experiment in which we measured the light intensity (photosynthetically active radiation; PAR) of 10 replicates of each treatment (total n = 70), positioned randomly across the two shelves (set up as in Figure C1 with conditions as described in the main text). PAR was measured with a Hobo Micro Station data logger and PAR sensor (Hoskin Scientfic, Edmonton, AB, Canada). We tested the effects of light intensity treatment, shelf, and their interaction on measured light intensity (PAR) using a two-way ANOVA (R function *aov*). A log-transformation was performed on the data prior to analyses due to non-normality.

Results

PAR (log-transformed) was not significantly different on the top shelf compared to the bottom shelf (Figure D1; two-way ANOVA, $F_{1,56} = 2.00$, $p = 0.16$). However, there was a significant main effect of treatment (Figure D1; two-way ANOVA, $F_{6,56} = 1387.67$, $p < 2.2 \times 10^{-16}$), and a significant interaction between shelf and treatment (Figure D1; two-way ANOVA, $F_{6,56} = 7.77$, $p = 4.22 \times 10^{-6}$). All light intensity treatments were significantly different, with each successively dimmer light intensity treatment having significantly lower PAR than the one before it (Figure D1; Tukey-Kramer post hoc tests). The interaction appeared to be largely due to a difference between the top and bottom shelf in the L_0 light intensity treatment. When the L_0 treatment was omitted from the analysis, the significant effect of treatment remained (two-way ANOVA, $F_{5,48} = 1487.11$, $p < 2.2 \times 10^{-16}$), as did the non-significant effect of shelf (two-way ANOVA, $F_{1,48} = 1.80$, $p = 0.19$). However, there was no longer a significant interaction between shelf and light intensity treatment (two-way ANOVA, $F_{5,48} = 0.95$, $p = 0.46$).

Conclusions

This ancillary experiment demonstrated that the light intensities of the treatments were not only significantly different from one another, they also closely matched their putative relative values for the six treatments in the $\log_2$-series (i.e., L_1 to $L_{1/32}$; see Figure D1), and were therefore suitable as a means of effecting caloric restriction in a precise manner. Moreover, the PAR values for the different treatments, ranging from 339 µmol m^{-2} s^{-1} for L_1 to 4 µmol m^{-2} s^{-1} for L_0 when averaged across shelves, spanned values of light intensity that are relevant to variation in growth rate and therefore plant metabolism (e.g., Docauer (1983) reported a half-saturation constant (i.e., Michaelis constant) of 35 µmol m^{-2} s^{-1} for *L. minor* plants grown at 28 °C).

We note that the 'no light' treatment, L_0, did not totally exclude light. This was not due to instrument error, as the PAR sensor gave a true zero when in complete darkness. Rather, we suspect it was due to a small amount of light that reached the underside of the (clear, non-zero thickness) outer lid from below. At any rate, the L_0 treatment had a much lower PAR than even the $L_{1/32}$ treatment (12 µmol m^{-2} s^{-1}, averaged across shelves).

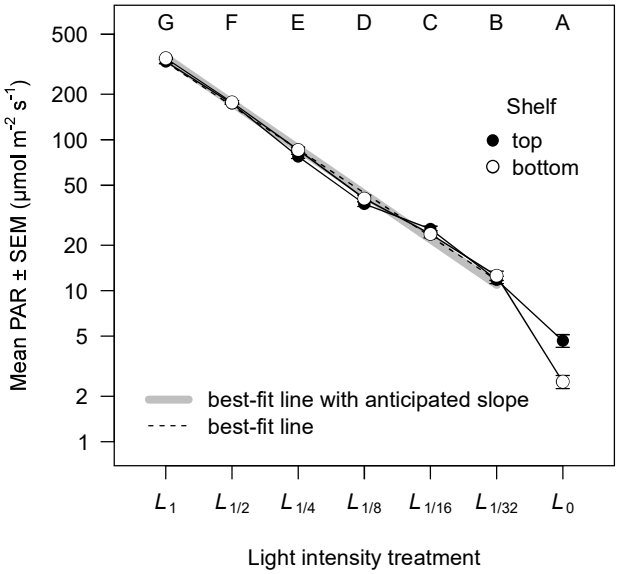

Figure D1. Interaction plot for mean photosynthetically active radiation (PAR in µmol m^{-2} s^{-1}; note logarithmic vertical axis, used to render equal *proportional* changes in PAR with equal magnitude) as a function of light intensity treatment and shelf, with the latter distinguished by symbols (black = top shelf; white = bottom shelf). Points and error bars are means ± 1 standard error of the mean (SEM), though some of the error bars are obscured because their extent was small relative to the size of the points. Treatments with no letters in common were significantly different; i.e., all light intensity treatments were significantly different from all others. Because the light intensity treatments L_1 to $L_{1/32}$ followed a putative $\log_2$ series, we anticipated that PAR should decrease by a factor of half between subsequent dimmer light intensity treatments, and further that the relationship between PAR (plotted on a logarithmic axis) versus light intensity treatment should be a straight line. To help assess this, for light intensity treatments L_1 to $L_{1/32}$, the thick grey line shows the best-fit line when the slope was fixed at the anticipated value and dashed line shows the best-fit line when this restriction was relaxed. There were 10 replicates per light intensity treatment, divided (top shelf / bottom shelf) 4/6 for L_0, 6/4 for $L_{1/2}$, 5/5 for $L_{1/4}$ to $L_{1/16}$, 3/7 for $L_{1/32}$ and 7/3 for L_0 (total n = 70).

Appendix E: Growth medium temperature as a function of light intensity treatment

Methods

We conducted a second ancillary experiment to determine whether light intensity treatments altered the growth medium temperature, as lifespan and other demographic traits are highly temperature dependent (specifically, plants live longer at lower temperatures; Körner, 1999; Nobis & Schweingruber, 2013; Paiha, 2021; Rosbakh & Poschlod, 2018; Wangermann & Ashby, 1951). To this end, we set up inner and outer containers, as in Figure C1. There were five replicates per treatment-by-shelf combination, positioned randomly (total $n = 70$). We allowed the temperature of the 4 mL of liquid within the containers to equilibrate for 8 hours after the start of the light phase, and then measured their temperature with a 'lollipop' thermometer (cat. no. 15079712, Fisher Scientific, Waltham, MA, USA). We tested the effects of light intensity treatment, shelf, and their interaction on growth medium temperature using a two-way ANOVA (R function *aov*).

Results

Growth medium temperature was significantly greater on the top shelf compared to the bottom shelf (Figure E1; two-way ANOVA, $F_{1,56} = 26.79$, $p = 3.18 \times 10^{-6}$). There was also a significant effect of light intensity treatment (Figure E1; two-way ANOVA, $F_{6,56} = 3.18$, $p = 0.0094$). The interaction between shelf and light intensity treatment was not significant (Figure E1; two-way ANOVA, $F_{6,56} = 0.76$, $p = 0.60$). The significant differences among light intensity treatments were driven by the L_0 treatment (Figure E1; Tukey-Kramer post hoc tests on pairs of light intensity treatments). When that treatment was omitted from the analysis, there was no significant effect of light intensity treatment (two-way ANOVA, $F_{5,48} = 1.20$, $p = 0.32$), nor a significant interaction between shelf and light intensity treatment (two-way ANOVA, $F_{5,48} = 0.48$, $p = 0.79$), though the significant main effect of shelf remained (two-way ANOVA, $F_{1,48} = 25.11$, $p = 7.77 \times 10^{-6}$).

Conclusions

This ancillary experiment detected no significant effect of light intensity treatment on growth medium temperature for treatments L_1 to $L_{1/32}$; however, the growth medium temperature in the treatment with a foil disc, L_0, was significantly cooler than in the other treatments. Thus, while we continued to include the L_0 treatment in Experiment 1, we cannot disentangle the effects of temperature and light for that treatment. The finding that temperature varied with shelf prompted us to re-randomize tray position daily in the main experiments; therefore, subsequent analyses in the main text relating to Experiments 1 and 2 did not involve shelf.

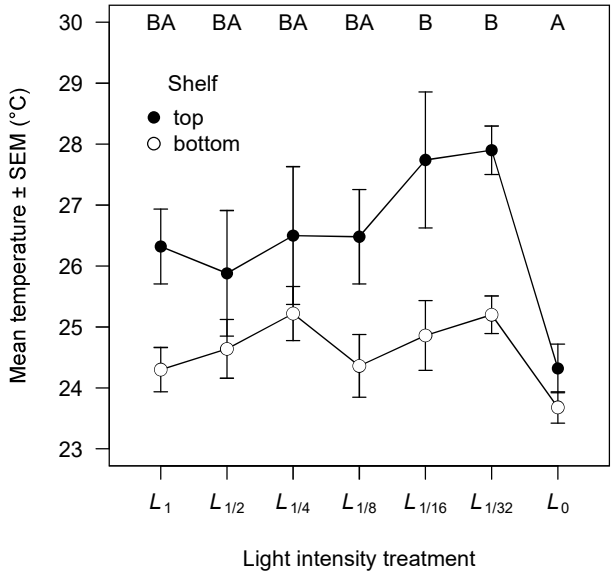

Figure E1. Interaction plot for mean temperature of growth medium in petri dishes (in °C) as a function of light intensity treatment and shelf, with the latter distinguished by symbols (black = top shelf; white = bottom shelf). Points and error bars are means ± 1 standard error of the mean (SEM). Treatments with no letters in common were significantly different; treatments with at least one letter in common were not significantly different. There were 10 replicates per light intensity treatment, divided equally among the top and bottom shelves (total n = 70).

Appendix F: Frond surface area

Methods

To determine whether there was any variation in plant size across light intensity treatments, after plant death (/experiment termination) we carefully flattened the plants, and then photographed them with no offspring attached, using a microscope-mounted digital camera (Clemex Technologies Inc., Longueuil, QC, Canada). The images were used to measure plants' surface areas using Matlab code developed by Ankutowicz & Laird (2018a, 2018b).

Plants were very delicate at this stage. Fifty-three plants were damaged during this process in Experiment 1, and did not yield usable images (L_1: n = 16; $L_{1/2}$: n = 23, $L_{1/4}$: n = 28; $L_{1/8}$: n = 26; $L_{1/16}$: n = 25; $L_{1/32}$: n = 21; L_0: n = 26; total n = 165). We used a one-way ANOVA to test the effects of light intensity on frond surface area (R function *aov*), and assessed ANOVA assumptions with residual-by-predicted plots and normal quantile-quantile plots.

In Experiment 2, there were 78 plants damaged during photographing, which did not yield usable images (L_1: n = 51; $L_{1/4}$: n = 77; total n = 128). We used a t-test to examine the effect of light intensity on frond surface area (R function *t.test*), and assessed model assumptions as in Experiment 1.

Results

Fronds in the seven light intensity treatments of Experiment 1 did not differ significantly in terms of surface area (Figure F1; one-way ANOVA, $F_{6,158} = 1.02$, $p = 0.42$).

Surface area of fronds in the two light intensity treatments of Experiment 2 did not differ significantly (Figure F2; t-test, $t_{126} = -1.09$, $p = 0.28$).

Conclusions

Light intensity did not affect frond surface area in the two experiments.

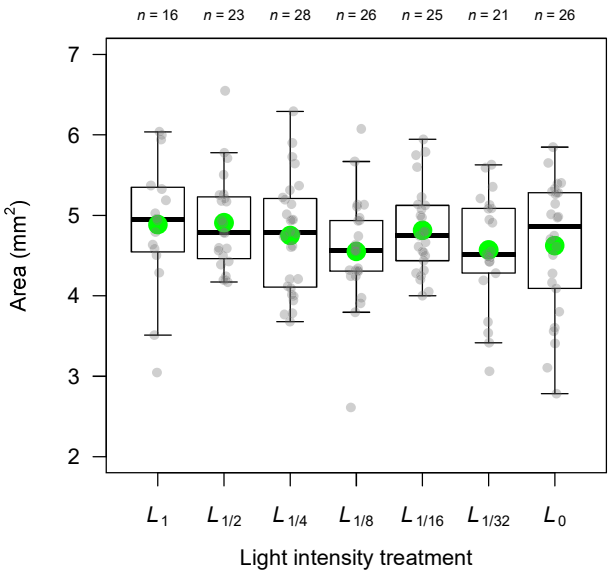

Figure F1. Box-and-whisker plot indicating frond area in mm^2 for the seven light intensity treatments in Experiment 1 (brighter to the left, dimmer to the right). Sample sizes (*n*) are shown above the panel. The thick horizontal line and the green point in each box represent the median and mean, respectively. The bottom and top of each box represent the first quartile (Q_1) and third quartile (Q_3), respectively. The lower whisker associated with each box represents the smallest value that is no less than $Q_1 - 1.5 \times IQR$, where $IQR = Q_3 - Q_1$ (i.e., the interquartile range). The upper whisker associated with each box represents the largest value that is no greater than $Q_3 + 1.5 \times IQR$. All data points are shown in grey with a slight horizontal jitter to make them easier to distinguish. Area was not significantly different among any of the light intensity treatments.

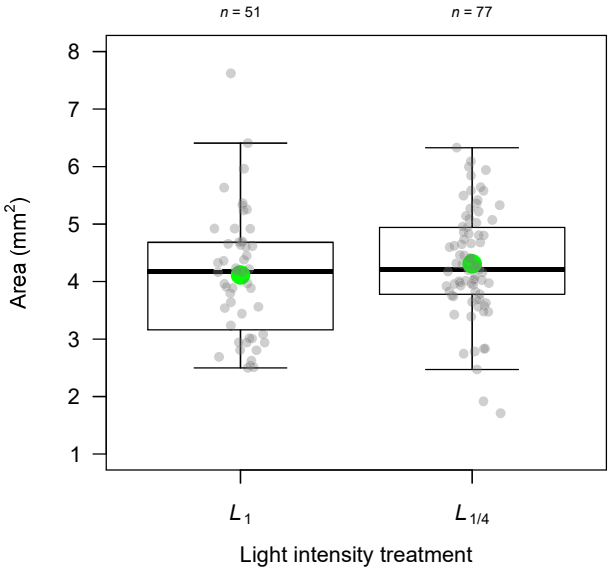

Figure F2. Box-and-whisker plot indicating frond area in mm^2 for the two light intensity treatments in Experiment 2. Sample sizes (*n*) are shown above the panel. The thick horizontal line and the green point in each box represent the median and mean, respectively. The bottom and top of each box represent the first quartile (Q_1) and third quartile (Q_3), respectively. The lower whisker associated with each box represents the smallest value that is no less than $Q_1 - 1.5 \times IQR$, where $IQR = Q_3 - Q_1$ (i.e., the interquartile range). The upper whisker associated with each box represents the largest value that is no greater than $Q_3 + 1.5 \times IQR$. All data points are shown in grey with a slight horizontal jitter to make them easier to distinguish. Area was not significantly different between the treatments.

Appendix G: Quantitative analysis of lifespan-versus-light intensity relationship

We assumed that metabolic rate relates to light intensity according to the Michaelis-Menten equation:

$$[metabolic\ rate] = \frac{p[light\ intensity]}{q + [light\ intensity]} \quad [G1]$$

where p is the asymptotic metabolic rate at high light intensity and q is the Michaelis constant.

We further assumed that lifespan relates to metabolic rate according to a power law:

$$\log[lifespan] = u - v \log[metabolic\ rate] \quad [G2]$$

where v is the power law's exponent, and u is a constant.

Putting these two assumptions together yields a predicted relationship between lifespan and light intensity:

$$\log[lifespan] = u - v \log\left(\frac{p[light\ intensity]}{q + [light\ intensity]}\right) \quad [G3]$$

This can be rearranged as the following:

$$\log[lifespan] = u - v \log p - v \log\left(\frac{[light\ intensity]}{q + [light\ intensity]}\right) \quad [G4]$$

Because $u - v \log p$ is a constant, we redefine that quantity as w, which is the asymptotic log lifespan at high light intensity:

$$\log[lifespan] = w - v \log\left(\frac{[light\ intensity]}{q + [light\ intensity]}\right) \quad [G5]$$

Appendix H: Quantitative analysis of temporal scaling of survival

If two survivorship functions, $l_1(t)$ and $l_2(t)$, have the same shape, such that $l_1(t)$ can be stretched or compressed along the time (t) axis to attain $l_2(t)$ (and vice versa), then $l_2(t) = l_1(t/\lambda)$, where λ is a dimensionless scale factor (i.e., a constant) (Stroustrup et al., 2016).

Per Pletcher et al. (2000), the mean lifespans, V_1 and V_2, associated with the survivorship functions $l_1(t)$ and $l_2(t)$, respectively, are given by

$$V_1 = \int_0^\infty l_1(t)dt \quad \text{[H1]}$$

$$V_2 = \int_0^\infty l_2(t)dt \quad \text{[H2]}$$

Thus, mean lifespan is equivalent to the area under the survivorship curve. Substituting $l_2(t) = l_1(t/\lambda)$ into the equation for V_2, gives

$$V_2 = \int_0^\infty l_1(t/\lambda)dt \quad \text{[H3]}$$

We can define $u = t/\lambda$, so that $\frac{du}{dt} = \frac{1}{\lambda}$. Then,

$$V_2 = \int_0^\infty l_1(u)\lambda du = \lambda \int_0^\infty l_1(u)du = \lambda V_1 \quad \text{[H4]}$$

(Note that the limits on the integral do not change when integrating with respect to u instead of t. The lower limit, 0, remains 0 because when $t = 0$, $u = t/\lambda = 0$. The upper limit, ∞, remains ∞ because as $t \to \infty$, so too does $u \to \infty$.)

Thus, $\lambda = V_2/V_1$ is equivalent to the ratio of the mean lifespans (Stroustrup et al., 2016). Intuitively, if survivorship curve l_2 is stretched horizontally by a factor of λ relative to l_1, then the mean lifespan associated with l_2 will increase λ-fold relative to mean lifespan associated with l_1**.** This is fortuitous, because it implies that if two cohorts have survivorship curves that are temporally scaled relative to one another when plotted against absolute age (e.g., in days), then those same survivorship curves plotted against *relative* age (i.e., absolute age divided by the mean absolute lifespan of their respective cohorts) will coincide.

To see why this is so, we can define $l_1'(t) = l_1(V_1 t)$ and $l_2'(t) = l_2(V_2 t)$. Both $l_1'(t)$ and $l_2'(t)$ have mean lifespans of 1, and are equivalent to plotting the survivorship curves against relative age. We can substitute $V_2 = \lambda V_1$ (derived above) into the equation for $l_2'(t)$ to get

$$l_2'(t) = l_2(\lambda V_1 t) \quad \text{[H5]}$$

Then we can apply the definition of $l_2(t) = l_1(t/\lambda)$ to get

$$l_2'(t) = l_1(\lambda V_1 t/\lambda) = l_1(V_1 t) = l_1'(t) \quad \text{[H6]}$$

This further implies that if two survivorship curves are temporally scaled relative to each other, they will have the same distribution of relative age-at-death. Similar to the approach of Stroustrup et al. (2016), this can be tested for empirical data using a non-parametric Kolmogorov-Smirnov (KS) test.

In this approach, a *non*-significant test result is consistent with curves arising from the same underlying distribution. With this in mind, before conducting the KS test on Experiment 2, we used Experiment 1's L_1 and $L_{1/4}$ lifespan distribution data to estimate the critical value of the KS test statistic, D_{crit}, that would provide no less than the typical target statistical power of 0.8 when applied to Experiment 2's sample sizes. To effect this, we ran 10,000 bootstrap replicates in which we randomly sampled, with replacement, 112 lifespans from each of Experiment 1's L_1 and $L_{1/4}$ treatments, converted them into relative lifespans, and then performed a KS test on each pair of simulated samples (n = 112 being the initial sample size per treatment in Experiment 2). The estimated value of D_{crit} = 0.1339 was the value that at least 80% of the bootstrap samples' KS D-values were greater than, including ties (Figure H1a). In an attempt to be more conservative, we re-ran the above analysis for the *realized* final sample sizes of Experiment 2 (n = 102 and 104 for L_1 and $L_{1/4}$, respectively); this gave an estimated value of D_{crit} = 0.1420 (Figure H1b). This actually turned out to be greater than the initial estimate, due to the presence of far fewer ties (contrast Figures H1b and H1a). Thus, we used the more conservative initial estimate of D_{crit} = 0.1339 in Experiment 2.

In this approach, D_{crit} was less than it would have been for these same sample sizes with the significance level, α, fixed to its typical value of 0.05. We considered this an acceptable cost to attain the target statistical power because, to reiterate, a *non*-significant test would affirm the presence of temporal scaling – counter to most hypothesis tests, in which a *rejection* of the statistical null hypothesis provides support for the scientific hypothesis in question. In this manner, our approach makes the test much more conservative than simply testing whether $p \leq 0.05$. That being said, the ideal experimental scenario would be one where both the Type I and Type II error rates are kept below some desired maxima. To that end, we echo Stroustrup et al.'s (2016) call for even larger sample sizes than we used in Experiment 2 to reduce the chances of erroneously rejecting a true null hypothesis, while simultaneously keeping the statistical power high. (But, we emphasize that we did not falsely reject the null hypothesis in this instance, because the KS test in Experiment 2 did not reject the null hypothesis in the first place; see main text for test results.)

Stroustrup et al. (2016) note that, for mutually temporally scaled survivorship functions, the distribution of the residuals of mean log(lifespan) also overlap. This makes sense – a horizontal *stretch* of λ on a t-axis is equivalent to a horizontal *translation* of log(λ) on a log(t)-axis. However, we focus on the first perspective (i.e., comparing distributions of relative age-at-death) because it provides a clear and intuitive link with our method of displaying our survival data (Figures 2b and 4b).

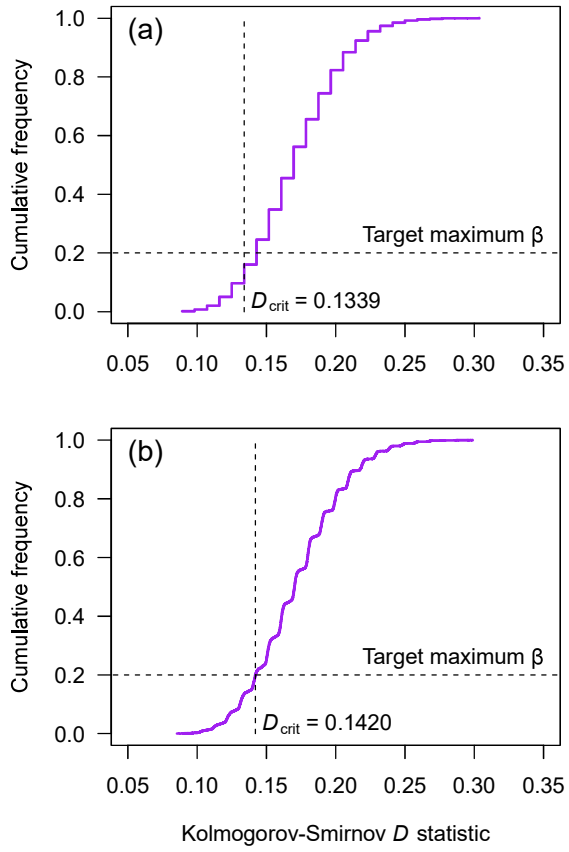

Figure H1. Empirical cumulative distribution functions of the Kolmogorov-Smirnov *D* statistic, calculated for bootstrapped relative lifespan distributions from the L_1 and $L_{1/4}$ treatments from Experiment 1, when applied to the (a) initial or (b) final sample sizes from those same treatments in Experiment 2. The dashed horizontal lines correspond to the target maximum value of β of 0.2 (corresponding to a target *minimum* statistical power of $1 - \beta = 0.8$). The dashed vertical lines are the estimates of D_{crit}; i.e., the values that at least 80% of the bootstrap samples' *D*-values were greater than, including ties. We used the lesser (i.e., more conservative) of these, $D_{crit} = 0.1339$, for the KS test in Experiment 2.

Appendix I: Quantitative analysis of temporal scaling of reproduction

In addition to survival (Appendix H), the temporal scaling framework can also be applied to reproduction. To do this we considered reproduction as a survival-like process, taking the perspective of the collective group of offspring born to each individual (Baudisch & Stott, 2019). Thus, an individual starts life with all its future offspring 'yet to be born'; this total then decrements with the birth of each subsequent offspring, eventually reaching zero. Figure I1a and Figure I2a show the number of offspring to be born versus absolute age for all focal plants in Experiments 1 and 2, respectively. Reproduction typically occurred steadily over plants' lives, with plants in dimmer light treatments living longer and producing slightly more offspring, in agreement with panels (a) and (b), respectively, of Figures 1 and 3.

Analogous to the phenomenon of population survival, where the cumulative number of individuals surviving to a given age is divided by the population size to get a population survivorship curve, an individual's cumulative number of offspring not yet born at a given age can be divided by that individual's total number of offspring to get an individual reproduction curve; both of these types of curves deal with proportions that start at one and decrease, monotonically, to zero. (We note that Baudisch and Stott (2019) instead consider cumulative reproduction to *increase* monotonically from zero to one – the choice is simply a matter of whether one chooses to focus on offspring born or yet to be born.) We emphasize that a survivorship curve is only useful at the population level – i.e., because individuals only die once (an *individual's* survivorship curve, were one to be constructed, would simply be one from birth to death and zero thereafter). On the other hand, because reproduction can potentially occur at multiple ages over an individual's lifetime, reproduction curves are also relevant at the individual level.

As in the survival context, in the reproduction context, absolute age can be converted to relative age. In terms of population survival, relative age is calculated by dividing absolute age by the mean lifespan of the relevant cohort. In terms of individual reproduction, relative age is calculated by dividing absolute age by an analogue of mean lifespan – specifically, the age of the individual of interest at the birth of an average offspring (Baudisch & Stott 2019). Thus, if an individual has a total of three offspring at absolute ages 2, 3, and 7 (arbitrary units), the corresponding relative ages at the time of the births of the offspring are $2/[(2 + 3 + 7)/3] = 0.5$, $3/[(2 + 3 + 7)/3] = 0.75$, and $7/[(2 + 3 + 7)/3] = 1.75$, which have a mean of $(0.5 + 0.75 + 1.75)/3 = 1$. Thus, relative ages can be calculated for the birth of every offspring of every individual.

The two operations discussed above (converting the number of offspring to be born into a proportion, and converting absolute age to relative age) have the effect of standardizing inter-individual variation in total reproduction and duration of reproduction. Having done this, similar to the approach of Stroustrup et al. (2016), the relative ages associated with every offspring can be aggregated by experimental treatment. If there is temporal scaling in terms of reproduction, the resulting curves should coincide. This was indeed the case for light intensity treatments in Experiments 1 and 2 (Figures I1b and I2b, respectively). Note that because individuals die once but produce multiple offspring, the overall sample sizes were considerably larger for the analysis of reproductive temporal scaling than they were for temporal scaling of survival (n = 1840 in Experiment 1 and n = 1912 in Experiment 2).

As with temporal scaling of survival (Appendix H), we used the results of Experiment 1 to inform the statistical analysis of the temporal scaling of reproduction in Experiment 2. Thus, we ran 10,000 bootstrap replicates in which we randomly sampled, with replacement, 849 and 1063 relative ages from Experiment 1's L_1 and $L_{1/4}$ treatments, respectively, re-standardized them by the means of the samples, and then performed a Kolmogorov-Smirnov test on each pair (n = 849 and n = 1063 being the total number of offspring produced in Experiment 2 in treatments L_1 and $L_{1/4}$, respectively). The provisional estimated value of D_{crit} = 0.06972 was the value that at least 80% of the bootstrap samples' KS D-values were greater than, including ties (Figure I3). However, because the sample size of offspring was so large, leading to high power, this provisional value turned out to be *greater* than the critical value when using a KS test with the typical significance level of α = 0.05. Thus, for the analysis of Experiment 2's data, given in Figure I2b, we simply did a straight KS test. This test revealed no significant difference in the distributions of relative age (Kolmogorov-Smirnov test, D = 0.029, n = 1912, p = 0.83), consistent with CR-mediated reproductive temporal scaling in Experiment 2 (Figure I2b).

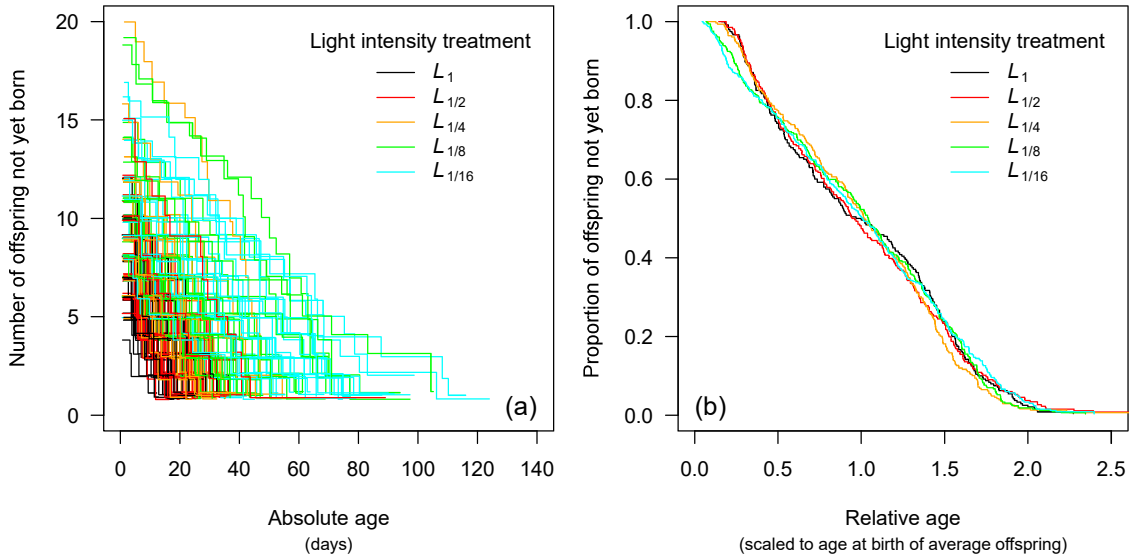

Figure I1. (a) Number of offspring not yet born versus absolute age in days, and (b) proportion of offspring not yet born versus relative age, scaled to the age at birth of an average offspring, in Experiment 1 (the 218 focal individuals in Experiment 1 produced 1840 offspring in total). Note that (a) has a subtle horizontal and vertical jitter to better visualize the data in the presence of many overlapping lines. In (a), each line represents the trajectory of offspring production for an individual focal plant; in (b), the trajectories are aggregated by light intensity treatment. Colours represent the five brightest light intensity treatments (black = L_1; red = $L_{1/2}$; orange = $L_{1/4}$; green = $L_{1/8}$; cyan = $L_{1/16}$). $L_{1/32}$ and L_0 are not given in either panel due to the experiment being terminated before all the plants had died (such that the number of offspring not yet born and the relative age could not be calculated for every experimental subject).

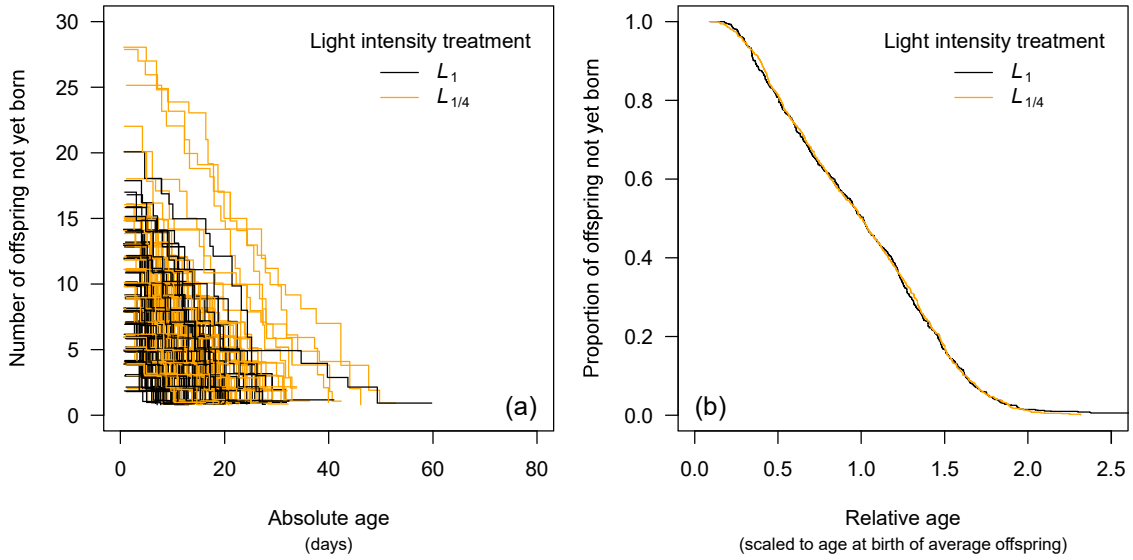

Figure I2. (a) Number of offspring not yet born versus absolute age in days, and (b) proportion of offspring not yet born versus relative age, scaled to the age at birth of an average offspring, in Experiment 2 (the 206 focal individuals in Experiment 2 produced 1912 offspring in total). Note that (a) has a subtle horizontal and vertical jitter to better visualize the data in the presence of many overlapping lines. In (a), each line represents the trajectory of offspring production for an individual focal plant; in (b), the trajectories are aggregated by light intensity treatment. Colours represent the two light intensity treatments (black = L_1; orange = $L_{1/4}$).

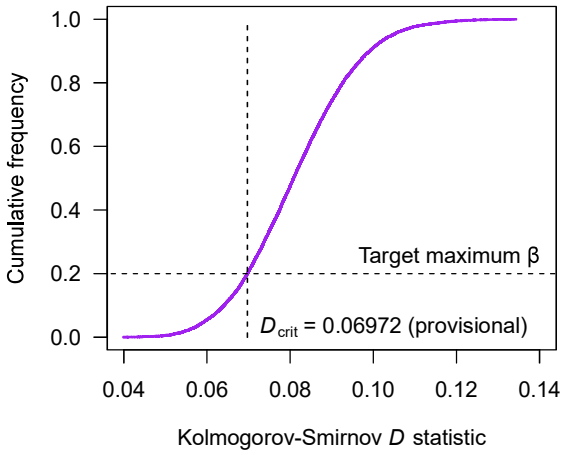

Figure I3. Empirical cumulative distribution function of the Kolmogorov-Smirnov *D* statistic, calculated for bootstrapped relative age distributions (scaled to age at birth of average offspring) from the L_1 and $L_{1/4}$ treatments from Experiment 1, when applied to the final sample sizes (total number of offspring) from those same treatments in Experiment 2. The dashed horizontal line corresponds to the target maximum value of β of 0.2 (corresponding to a target *minimum* statistical power of $1 - \beta = 0.8$). The dashed vertical line is the estimate of D_{crit}; i.e., the value that at least 80% of the bootstrap samples' *D*-values were greater than, including ties. Because this provisional value of 0.06972 was greater than the D_{crit} for a standard KS test (0.06251), we elected to simply perform a standard KS test on Experiment 2's data.

References

Adler, M.I. & Bonduriansky, R. (2014) Why do the well-fed appear to die young? A new evolutionary hypothesis for the effect of dietary restriction on lifespan. *Bioessays*, 36, 439-450.

Anisimov, V.N., Zabezhinski, M.A., Popovich, I.G., Piskunova, T.S., Semenchenko, A.V., Tyndyk, M.L. et al. (2011) Rapamycin increases lifespan and inhibits spontaneous tumorigenesis in inbred female mice. *Cell Cycle*, 10, 4230-4236.

Ankutowicz, E.J. & Laird, R.A. (2018a) Offspring of older parents are smaller—but no less bilaterally symmetrical—than offspring of younger parents in the aquatic plant *Lemna turionifera*. *Ecology and Evolution*, 8, 679-687.

Ankutowicz, E.J. & Laird, R.A. (2018b) Offspring of older parents are smaller—but no less bilaterally symmetrical—than offspring of younger parents in the aquatic plant *Lemna turionifera*, Dryad Data Repository.

Barks, P.M. & Laird, R.A. (2015) Senescence in duckweed: age-related declines in survival, reproduction and offspring quality. *Functional Ecology*, 29, 540-548.

Baudisch, A. & Stott, I. (2019) A pace and shape perspective on fertility. *Methods in Ecology and Evolution*, 10, 1941-1951.

Bjedov, I., Toivonen, J.M., Kerr, F., Slack, C., Jacobson, J., Foley, A. et al. (2010) Mechanisms of life span extension by rapamycin in the fruit fly *Drosophila melanogaster*. *Cell Metabolism*, 11, 35-46.

Blagosklonny, M.V. (2006) Aging and immortality: quasi-programmed senescence and its pharmacologic inhibition. *Cell Cycle*, 5, 2087-2102.

Blagosklonny, M.V. (2008) Aging: ROS or TOR. *Cell Cycle*, 7, 3344-3354.

Blagosklonny, M.V. & Hall, M.N. (2009) Growth and aging: a common molecular mechanism. *Aging*, 1, 357.

Chung, K.W. & Chung, H.Y. (2019) The effects of calorie restriction on autophagy: Role on aging intervention. *Nutrients*, 11, 2923.

Docauer, D.M. (1983) *A nutrient basis for the distribution of the Lemnaceae*. Doctoral dissertation thesis, University of Michigan, Ann Arbor, MI.

Fabrizio, P., Pozza, F., Pletcher, S.D., Gendron, C.M. & Longo, V.D. (2001) Regulation of longevity and stress resistance by Sch9 in yeast. *Science*, 292, 288-290.

Gems, D. & Partridge, L. (2013) Genetics of longevity in model organisms: debates and paradigm shifts. *Annual Review of Physiology*, 75, 621-644.

González, A., Hall, M.N., Lin, S.-C. & Hardie, D.G. (2020) AMPK and TOR: the yin and yang of cellular nutrient sensing and growth control. *Cell Metabolism*, 31, 472-492.

Jia, K., Chen, D. & Riddle, D.L. (2004) The TOR pathway interacts with the insulin signaling pathway to regulate *C. elegans* larval development, metabolism and life span. *Development*, 131, 3897-3906.

Kapahi, P., Zid, B.M., Harper, T., Koslover, D., Sapin, V. & Benzer, S. (2004) Regulation of lifespan in *Drosophila* by modulation of genes in the TOR signaling pathway. *Current Biology*, 14, 885-890.

Körner, C. (1999) Alpine plants: stressed or adapted?, Pages 297-311 *in* M. C. Press, J. D. Scholes&M. G. Barker, eds. Physiological Plant Ecology. Cambridge, UK, Cambridge University Press.

Le Bourg, É. (2010) Predicting whether dietary restriction would increase longevity in species not tested so far. *Ageing Research Reviews*, 9, 289-297.

Loewith, R. & Hall, M.N. (2011) Target of rapamycin (TOR) in nutrient signaling and growth control. *Genetics*, 189, 1177-1201.

Lemaître, J.-F., Moorad, J., Gaillard, J.-M., Malakov, A.A. & Nussey, D.H. (2024) A unified framework for evolutionary genetic and physiological theories of aging. *PLoS Biology*, 22, e3002513.

Nakagawa, S., Lagisz, M., Hector, K.L. & Spencer, H.G. (2012) Comparative and meta-analytic insights into life extension via dietary restriction. *Aging Cell*, 11, 401-409.

Nobis, M.P. & Schweingruber, F.H. (2013) Adult age of vascular plant species along an elevational land-use and climate gradient. *Ecography*, 36, 1076-1085.

Paiha, A. (2021) *Senescence in duckweed: An interspecific comparison and the influence of temperature*. Masters Thesis thesis, University of Lethbridge (Canada), Lethbridge, AB.

Pletcher, S.D., Khazaeli, A.A. & Curtsinger, J.W. (2000) Why do lifespans differ? partitioning mean longevity differences in terms of age-specific mortality parameters. *The Journals of Gerontology Series A: Biological Sciences and Medical Sciences*, 55, B381-B389.

Powers, R.W., Kaeberlein, M., Caldwell, S.D., Kennedy, B.K. & Fields, S. (2006) Extension of chronological life span in yeast by decreased TOR pathway signaling. *Genes & Development*, 20, 174-184.

Rosbakh, S. & Poschlod, P. (2018) Killing me slowly: Harsh environment extends plant maximum life span. *Basic and Applied Ecology*, 28, 17-26.

Saxton, R.A. & Sabatini, D.M. (2017) mTOR signaling in growth, metabolism, and disease. *Cell*, 168, 960-976.

Stroustrup, N., Anthony, W.E., Nash, Z.M., Gowda, V., Gomez, A., López-Moyado, M.E. et al. (2016) The temporal scaling of *Caenorhabditis elegans* ageing. *Nature*, 530, 103-107.

Vellai, T., Takacs-Vellai, K., Zhang, Y., Kovacs, A.L., Orosz, L. & Müller, F. (2003) Influence of TOR kinase on lifespan in *C. elegans*. *Nature*, 426, 620-620.

Wangermann, E. & Ashby, E. (1951) Studies in the Morphogenesis of Leaves. VII Part I. Effects of Light Intensity and Temperature on the Cycle of Ageing and Rejuvenation in the Vegetation Life History of *Lemma minor*. *New Phytologist*, 50, 186-199.

Williams, G.C. (1957) Pleiotropy, natural selection, and the evolution of senescence. *Evolution*, 11, 398-411.